UNCLASSIFIED
SECURITY CLASSIFICATION OF THIS PAGE

(2)

REPORT DOCUMENTATION PAGE

DTIC FILE COPY

AD-A211 886 DTIC ELECTE SEP 05 1989 D

1b RESTRICTIVE MARKINGS	
2b DECLASSIFICATION / DOWNGRADING SCHEDULE	3 DISTRIBUTION / AVAILABILITY OF REPORT Approved for public release and sale; its distribution is unlimited.
4. PERFORMING ORGANIZATION REPORT NUMBER(S) Technical Report No. 68	5. MONITORING ORGANIZATION REPORT NUMBER(S)
6a NAME OF PERFORMING ORGANIZATION Case Western Reserve University	6b. OFFICE SYMBOL (If applicable)
6c. ADDRESS (City, State, and ZIP Code) Cleveland, Ohio 44106	7a. NAME OF MONITORING ORGANIZATION ONR Chemistry Program
	7b. ADDRESS (City, State, and ZIP Code) Arlington, Virginia 22217-5000
8a. NAME OF FUNDING / SPONSORING ORGANIZATION Office of Naval Research	8b. OFFICE SYMBOL (If applicable)
	9. PROCUREMENT INSTRUMENT IDENTIFICATION NUMBER Contract N00014-83-K-0343
8c. ADDRESS (City, State, and ZIP Code) Arlington, Virginia 22217-5000	10 SOURCE OF FUNDING NUMBERS

PROGRAM ELEMENT NO.	PROJECT NO.	TASK NO.	WORK UNIT ACCESSION NO
	NR359-451		

11. TITLE (Include Security Classification)
The Effects of Trace Anions on the Voltammetry of Single Crystal Gold Surfaces

12. PERSONAL AUTHOR(S)
B. D. Cahan, H. M. Villullas and E. B. Yeager

13a. TYPE OF REPORT	13b. TIME COVERED	14. DATE OF REPORT (Year, Month, Day)	15. PAGE COUNT
Technical Report	FROM 1988 TO 1989	August 18, 1989	31

16. SUPPLEMENTARY NOTATION

17. COSATI CODES		
FIELD	GROUP	SUB-GROUP

18. SUBJECT TERMS (Continue on reverse if necessary and identify by block number)
rotating disk electrode, hanging meniscus, single crystal electrodes, anion impurities.

19. ABSTRACT (Continue on reverse if necessary and identify by block number)

The development of a new technique for mounting single crystals as a Hanging Meniscus Rotating Disk (HMRD) electrode has facilitated the study of the effect of traces of anionic impurities on the voltammetry of gold single crystals. It is shown that the cause of most of the differences between voltammetry curves reported in the literature for the same crystal face is the presence in the solution of low levels (≈10^{-7} M) of Cl^- and $SO_4^{=}$ ions which were present in the original reagent. Variation of the rotation rate from 0-10,000 r.p.m. permitted a change of the effective concentrations of these impurities by a factor of ≈100. The resultant curves are compared to those produced by purposeful addition of these anions.

89 9 01141

20 DISTRIBUTION / AVAILABILITY OF ABSTRACT	21 ABSTRACT SECURITY CLASSIFICATION
☒ UNCLASSIFIED/UNLIMITED ☐ SAME AS RPT ☐ DTIC USERS	unclassified
22a NAME OF RESPONSIBLE INDIVIDUAL Ernest Yeager, Professor of Chemistry	22b TELEPHONE (Include Area Code) (216) 368-3626
	22c. OFFICE SYMBOL

DD FORM 1473, 84 MAR 83 APR edition may be used until exhausted
All other editions are obsolete

SECURITY CLASSIFICATION OF THIS PAGE
UNCLASSIFIED

OFFICE OF NAVAL RESEARCH

Research Contract N00014-83-K-0343

Technical Report No. 68

THE EFFECTS OF TRACE ANIONS ON THE VOLTAMMETRY OF SINGLE CRYSTAL GOLD SURFACES

by

B. D. Cahan, H. M. Villullas and E. B. Yeager

Prepared for Publication

in the

Journal of Electroanalytical Chemistry
and Interfacial Electrochemistry

Case Center for Electrochemical Sciences
and the Department of Chemistry
Case Western Reserve University
Cleveland, Ohio 44106-2699

18 August 1989

The Effects of Trace Anions on the Voltammetry of Single Crystal Gold Surfaces

B. D. Cahan, H. M. Villullas[1] and E. B. Yeager
Case Center for Electrochemical Sciences
and the Dept. of Chemistry,
Case Western Reserve University
Cleveland, Ohio 44106

[1]on leave from Depto de Fisicoquimica, Facultad de Ciencias Qimicas, U. N. C.,Cordoba, Argentina

Abstract

The development of a new technique for mounting single crystals as a Hanging Meniscus Rotating Disk (HMRD) electrode has facilitated the study of the effect of traces of anionic impurities on the voltammetry of gold single crystals. It is shown that the cause for most of the differences between voltammetry curves reported in the literature for the same crystal face is the presence in the solution of low levels ($\approx 10^{-7}$M) of Cl^- and $SO_4^=$ ions which were present in the original reagent. Variation of the rotation rate from 0–10,000 r.p.m. permitted a change of the effective concentrations of these impurities by a factor of ≈ 100. The resultant curves are compared to those produced by purposeful addition of these anions.

INTRODUCTION

An examination of the recent literature on the cyclic voltammetry of low index surfaces of gold single crystals shows that there are many conflicting reports about the number, relative size and shape of the peaks observed in various electrolytes . The main questions that appear to be central are the quality and/or perfection of the surface and the nature and purity of the electrolyte. For example, the published data and discussions relative to the < 111 > face [1–5] have variously attributed the observed differences to surface structure and preparation, nature of the relevant anions and "impurities". Figures 1a–1e show a representative sampling of such curves. Figures 2a–2d show similar curves for the < 100 > face. For the < 100 > [4–7] and < 110 > [8,9] faces the controversy is not as clearly documented as for the < 111 >, but significant differences are observable between published curves, even in different papers by the same author(s). From these examples it can be seen that controversy exists over the following:

1. whether or not ClO_4^- and F^- behave in a similar fashion, and whether either is specifically adsorbed on Au,
2. the validity of the "fingerprint" concept for identification of developed faces [10] and as a criterion for assessing crystalline perfection [11],
3. whether cycling into the oxide region removes or concentrates impurities,
4. whether cycling into the H_2 potential region damages the surface,
5. the effect of traces of anions, including Cl^- and $SO_4^=$, on the shape of the curves,
6. the effects of temperature, electrolyte concentration, and sweep limits on the values of the double layer capacity and the PZC [12,13],
7. the restructuring of the surface by recycling and the effect of anions on reconstruction.

Previous attempts at using single crystals in rotating disk arrangements [14,15] have relied on epoxy or Teflon shrouds to isolate and insulate the side surfaces of the crystals. These mounts are prone to leaks and contamination, and often suffer from difficulties with alignment of the desired face with respect to the axis of rotation. The development of the Hanging Meniscus Rotating Disk (HMRD) [16], which is a new method of mounting single crystals for use as rotating disk electrodes, has made possible the study of the effects of traces of impurities (such as Cl^- and SO_4^-) in a controlled, continuous and reversible manner.

EXPERIMENTAL

Single Crystal Preparation

Some of the crystals (< 100 >,< 110 > and < 111 >) were purchased from Metal Crystals and Oxides, Ltd., (Cambridge, England) as 6.0 × 6.0mm cylinders (5N purity). Others were prepared in this laboratory from Au which was chemically precipitated from $AuCl_3$ solutions with hydroxylamine hydrochloride several times, until the crystallites were shiny and self-adherent. The precipitated Au was washed repeatedly in dilute HCl, HNO_3 and H_2O before melting. The crystals were grown in clean graphite crucibles, and spark-cut to size. No special analysis of these crystals was done, but the ease of single crystal growth was used as a crude indicator of purity.

All crystals were mounted and oriented to better than 0.5° (typically 0.3°) using a modification of techniques developed by D. M. Zehner [17]. A miniature autocollimator was designed to align the polished surfaces optically to the X-ray track, and/or to the spark cutter. Special fixtures allowed alignment of the surfaces to the polishing wheel with similar precision and examination of the crystals on a metallograph between polishing steps. Mechanical polishing was done on a Buehler Whirlimet Attachment, using Microcut 1200 paper, followed by alumina down to 0.05 micron. Metallographic examination showed that diamond below 9 micron was unusable since it caused minute shavings to reattach to the surface, making tiny bumps of randomly oriented material which were not removable. Nylon was used with the alumina down to 1 micron to maintain physical flatness. Microcloth was used with 0.3 and 0.05 micron alumina, since the Nylon scratched the surface at those sizes. All alumina polishing was done with very dilute suspensions, flooding the surface with clean water to flush away *Au* shavings. This procedure maintains sharp angles at the edge of the crystal, allowing precise positioning of the meniscus when mounted in the HMRD holder.

After mechanical polishing, the surfaces were electropolished in a modified cyanide bath developed by Zehner [17] to remove physical damage, annealed in a tube furnace at 750° in *Ar* and monitored by perfection of the Laue spots. All of the crystals were cleaned anodically before each set of experiments to grow a visible thick oxide, followed by dissolution of the oxide in *HCl* [18] and rigorous washing in ultra-pure water produced by reverse osmosis and distillation under N_2 [19].

HMRD Mount

The HMRD was conceived as a combination of the pendant meniscus [20] and a rotating disk. The crystals were mounted in an adapter to a Pine rotator made from a Kel-F W. W. collet in a Kel-F nosepiece. Centering of the crystal within 0.001″ was easily possible. No external shroud for the crystal was used. The crystal was simply lowered until contact with the electrolyte was made (establishing the reference level) and raised to develop a hanging meniscus of the desired shape, using a dial gage to measure the height within 0.001″. The symmetry and small size of the mount allowed us to rotate at very high speeds (up to 10,000 r.p.m.) without visible turbulence or perturbation of the liquid surface. Measurements of the ferri-ferrocyanide couple showed that the system exhibits Levich behavior very closely with respect to the linearity and the slope of the i *vs.* $\omega^{1/2}$ curve [16]. The wetting of the side of the crystal was easily controlled by careful adjustment of the height of the meniscus, which was completely stable up to 3.0 mm.

Electrochemical Cell and Support Equipment

The electrochemical measurements were done in a conventional cell made of Pyrex with a lid of Teflon. The counter electrode was a gold sheet, separated by a glass frit. The reference was usually an SCE in a separate compartment connected to the main cell by a tube and stopcock bridge. A gold wire wrapped around the tube and dipping into both compartments served to decrease the series impedance of the reference electrode for transient stability and to reduce extraneous noise. All potentials are reported *vs.* SCE except as noted. A 1 mm gap between the rotating shaft and the lid was present, but purified N_2 flowed over the surface and helped prevent diffusion of air into the cell.

Measurements of the gold electrodes under static and rotating conditions were done using 0.01M and 0.1M $HClO_4$ and HF prepared from J. T. Baker Ultrex[1] or Seastar Chemicals[2] reagents using standard preparation techniques. These solutions were deaerated in the cell with N_2 before each run. From the analysis of the reagents supplied with the Ultrex acids, the minimum concentrations of Cl^- and $SO_4^=$ in the 0.1M $HClO_4$ are estimated to have been 2×10^{-7}M and 3×10^{-7}M respectively. For the 0.1 M HF the values are 1×10^{-7}M and 0.5×10^{-7}M. The water preparation system [19] does not utilize activated carbon filters or ion exchange resins (which introduce non-ionic electroactive species not detectable by simple conductivity measurements). This system produces water whose surface tension is within a fraction of a dyne/cm of ideal, and which gives no detectable Rayleigh line with laser scattering. The measured resistivity is between 15 and 17 Mohm. Most of the small residual is probably due to dissolved Pyrex and CO_2. We therefore estimate that the maximum ionic impurity level in the water is of the order of 10^{-8}M. Potentials were controlled by a Stonehart BC1200 potentiostat, which has built-in IR compensation and IR correction circuits. A PARC 175 Programmer was used for setting the potential. Most of the CV curves were recorded with an analog recorder. On some curves a small filter network was used with the recorder to minimize brush noise while rotating.

PROCEDURES AND RESULTS

Since the thickness of the effective diffusion layer for a RDE decreases with the square root of rotation rate, spinning the electrode (for a solution where impurities are present in trace amounts and therefore where adsorption is diffusion limited) is equivalent to increasing the effective concentration. Variation of sweep speed has a similar effect, but limitations imposed by practical sweep rates, noise level and recorder sensitivity precludes as wide a range of accessible values. Additionally, varying sweep speed not only requires a change of range on the recording device, but alters the shape of any peaks, including those involving species on the surface. [Note that a sweep rate of 5 μV/sec is required to achieve the same concentration effects as those obtained with a sweep rate of 50 mV/sec and a rotation rate of 10,000 r.p.m.] The use of the HMRD is thus equivalent to "reversible" contamination. The curves stay the same in size and shape *except for those parts affected by diffusion*. Traces of impurities which are intentionally added cannot usually be removed after addition to recheck the condition of the electrode surface.

Since the intent of this study was to look at the effects of impurities, we examined separately the effects of sweep rate, rotation rate and actual impurity concentration. Single crystal electrodes were cleaned, mounted and balanced and lowered into the electrolyte. After raising the meniscus, the electrodes were cycled briefly to check reproducibility and similarity to published curves. When steady state behavior was attained (this took from 2 to 25 cycles depending on the conditions), the electrode was rotated, usually in steps which doubled (or halved) the rotation rate at each step. Significant differences were observed between the curves at different rotation rates except for some runs at the lowest one or two spin rates. Identical curves were usually obtained before and after spinning. In some cases, particularly when excess Cl^- was added (see below), it took several cycles to reestablish the base curve. At times, the potential was cycled repeatedly into the H_2 evolution region (to -800 mV SCE). The only effects that were observed were a slight ($< 3\%$) increase in the first peaks. The steady-state curves were restored within 1-2 cycles after the lower potential

[1] Purified by vacuum distillation

[2] Purified by evaporation in a stream of inert carrier gas.

limit was reduced. Occasionally, a very small anodic peak(s) was observed for one cycle only after extended holding in the H_2 region. These were probably due to the UPD or to cathodic deposition of traces of cations whose concentration was too low to detect after one sweep.

< 100 > face

Figure 3a shows the curve obtained for a < 100 > face in 0.01M $HClO_4$ (Seastar) at 80 mV/sec with no rotation. Going clockwise around the curve from the cathodic limit, the following details can be observed:

1. There is a very small bump(A) at 570 mV SCE, ($Q <= 1.0\mu C/cm^2$) followed by a broad plateau (B) extending to 850 mV ($Q = 18\mu C/cm^2$).

2. The current then rises to a small sharp peak (C) at 900 mV and a second sharp peak (D) at 950 mV. A shoulder (E) is visible to the right of this peak.

3. This is followed by a broader peak (F) at 1035 mV.

4. This peak drops to a broader plateau in which there is a fourth broad peak (G) at 1225 mV followed by a rise to 1400 mV, at which point the sweep direction is reversed.

5. Oxidation continues but the rate drops rapidly to the zero crossing potential of approximately 1170 mV.

6. A large reduction peak (H) centered at 730 mV is followed by a sharp shoulder (I) at 640 mV and a broader shoulder (J) which ends at 470 mV.

7. The double layer region is wide, decreasing to a minimum (K) at 100 mV at which point the double layer capacity (estimated from the width of the curve) is about $40\mu F/cm^2$.

8. This is followed by a broad hump (L) which ends at −80 mV. The double layer capacity at more negative potentials is about $20 - 22\mu F/cm^2$.

It should be pointed out that the curve in Fig. 3a was obtained using both the IR correction and compensation capabilities of the BC1200 potentiostat. Significant differences are observed when this procedure is followed from the uncorrected and uncompensated curves. In our geometry, the value of the resistance of the electrolyte was approximately 260 ohms in 0.01M solution. This caused a shift of 20–30 mV for the peak potentials. Even more significantly, peak D is about 20% higher with IR compensation than without. This means that the exact shape of the curve will depend on the placement of the reference electrode as well as the purity of the electrolyte and the quality of the surface. [Not all of the figures utilized the correction/compensation method. Those that do will be so noted.]

Figure 3b shows a typical set of curves for different rotation rates with an expanded scale to provide higher resolution of fine structure. (Selected curves have been deleted from the original data set in this and subsequent figures for clarity). The curves for no rotation and for 50 and 100 r.p.m. are almost identical, showing only very small changes in peak F. Further increases in the rotation rate cause changes in the various features:

1. Processes A - F are gradually suppressed up to the isopotential point at 1045 mV. As peaks C and D are suppressed, they are smoothly shifted anodically. All of the suppressed charge is quantitatively recovered at higher potentials (see below).

2. Most of the recovered charge appears initially in a new peak F' (which may not be the same as F).

3. G disappears and/or is replaced by a plateau.

4. The onset of oxide reduction (H) shifts up to 20 mV more positive at higher rotation rates.

5. Processes I and J, which appear to be distinct and identifiable with processes D and C from window opening experiments, are also suppressed.

6. The start of L moves to more positive values of potential , but the endpoint is almost constant within 15 mV. The shape of L is clearly non-Langmuirian and is suggestive of a Temkin-like desorption process (21).

7. The curve at more negative potentials values drops slightly, probably because of residual traces of dissolved oxygen , whose transport is enhanced by rotation. Even in the presence of this reaction, the double layer capacitance remains at $22\mu F/cm^2$.

The effect of Cl^- on this system was studied by adding controlled amounts of dilute HCl with a micro-syringe. Two additions , the first up to 5×10^{-7}M Cl^- and the second to 2.5×10^{-6}M, were made and a set of rotations recorded. The curves which resulted from the first addition were generically almost identical to those shown in Figure 3b but they are shifted in rotation rate by a factor of two. For example, the curve at 200 r.p.m. in 5×10^{-7}M Cl^- corresponds to the curve at 400 r.p.m. in the original solution. Figure 4 shows the data set for the second addition. These curves also show the same generically shifted shapes, with a rotation factor above 4 and below 8. The curves at the highest two rotation rates, which have no correspondents in Figure 3b, show that the oxidation suppression reaches saturation and all of this charge before the isopotential point is now forced into a new peak F''. At the same time the peaks C and J are totally absent and the broad desorption peak L has reached a saturation limit, starting *immediately after* the end of peak I.

At this point, it is clear that the effects observed in Figure 3b as a function of rotation are identical to those caused by the intentional addition of Cl^- ions. It is not as clear where in the anodic sweep the ions are adsorbed since the adsorption is diffusion limited and most of the structure in the adsorption process is wiped out. These data are also complicated by the presence in the original solution of traces of $SO_4^=$ (as pointed out above) which is simultaneously adsorbing in a diffusion limited manner over this potential range. The characteristics of the desorption peaks for the two species are enough different that they can be resolved under some conditions, particularly at low concentrations and without stirring. Window opening experiments were done, with the negative limit set at −300 mV SCE (or −400) and the anodic limit stepped from 100 mV to 1400 mV in 100 mV steps at a number of rotation rates up to 10,000 r.p.m. The results for 0 and 10,000 r.p.m. (where saturation is observed) are shown in Figs. 5a and 5b and should be compared to the results for trace $SO_4^=$ in Fig. 10, given later. Between -100 mV and 50 mV, Cl^- adsorption is the primary process, and a single desorption peak is observed. Up to 600 mV the co-adsorption is the

only process, and the Cl^- ion is close to saturation at 10,000 r.p.m. but only has half coverage at 1000. From 600 to 900 mV additional Cl^- and $SO_4^=$ adsorbs on the positive and negative portions of the curve. Above 900 mV, where surface oxide forms, no additional anions adsorb or desorb. However, since oxides are present during the reverse sweep down to 500 mV, and Cl^- does not adsorb with the oxide present, the total Cl^- adsorbed is decreased.

The peak L has the appearance of a Temkin-type desorption [21] of the Cl^- with an r-factor of approximately 10. (The presence of the $SO_4^=$ complicates the analysis at higher coverages. Both anions may be desorbing simultaneously over part of the desorption potential range.) The baseline for this isotherm is sufficiently stable under rotation to allow integration under the curve, although there are small systematic errors which are difficult to estimate because of residual oxygen currents at potentials below $\approx$ 0 V and may include some current for the desorption of $SO_4^=$. The results of these integrations from Fig. 3b are shown plotted *vs.* the square root of rotation rate in Fig. 6a.

The integrals under the anodic curves of Fig. 3b from 600 mV to 1400 mV are the same (within 5%) for all rotation rates studied. The integrals under the same curves from 600 mV to the isopotential point at 1045 mV were also measured. Recognizing that the static curve of Fig. 3b is almost free of adsorbed anions we can take this curve as a baseline. Subtracting each subsequent curve from the base curve gives the amount of charge for oxide formation ($Q_o - Q_\omega$) which was suppressed by the action of the anions. These values are shown in Fig. 6b(1), plotted *vs.* the square root of rotation rate. Figure 6c shows this charge difference *vs.* the integrated charge under peak L. This line does not go through zero, and is indicative of the presence of the small but finite amount of residual impurity anions adsorbed from the unstirred solution. All of the suppressed charge appears after the isopotential point.

The results of the same integrations for the data of Fig. 4 (with 2.5×10^{-6}M HCl added) are shown in Fig. 7. Even when the Cl^- adsorption has reached saturation, the linearity of ($Q_o - Q_\omega$) *vs.* Q_{Cl^-} is maintained. [The small difference in slope between Figs. 6c and 7c may be due to a systematic shifting of the baseline in Fig. 4 or to the different ratio of Cl^- to $SO_4^=$.] A similar analysis of the suppression of reduction peaks I and J (which have been shown to be intimately related to peaks D and C) shows the same linearity, and the combined values for the two peaks are shown in Fig. 6b(2). Note that the integrals for I and J suppressed are completely resolved. It is very difficult to deconvolute the charge associated with peaks C, D and E in the anodic scan. It is tempting to assume that the results of the processes in peaks C and D are completely preserved during the subsequent oxidation (E, F and G) and reduction of the main portion of the oxide material (H). This would permit a more quantitative separation of the magnitude of peaks E, F and G.

It is clear from a comparison of Fig. 4 and Fig. 3b that most of the effects observed are a function of the presence of Cl^- . The exact role of the ion is not so clear yet. Certain observations can be made:

1. When saturation has been reached, the Cl^- desorption occurs immediately after the reduction of the oxide is completed. Therefore, it can be seen that the Cl^- must be present in some form during the entire oxidation-reduction cycle. It appears that it is somehow incorporated into the lattice, probably as some AuO_xCl_y or $Au(OH)_xCl_y$ species.

2. The presence of Cl^- causes inhibition of peaks A to E. Even at saturation a small residual charge at I persists (which may correspond to peak E which is hidden in the intermediate curves).

3. The amount of oxide suppressed is linearly related to the amount of Cl^- which is desorbed. This relationship holds for each of the individual peaks.

4. The proportionality between the effects of rotation rate in the presence of the two concentrations of intentionally added Cl^- permits us to establish approximately the concentration of Cl^- in the original solution as being in the range of $1 - 5 \times 10^{-7}$.

Figure 8 shows a set of curves for the < 100 > face under the same conditions as for Fig. 3b but at a sweep speed of 20 mV/sec. The scale had to be expanded considerably and the effects of residual oxygen are much more apparent at low potentials. The main differences are as follows:

1. Peaks C and D are considerably sharper than at 80 mV/sec. The potential of the onset of oxidation is the same but the peak potential is shifted as expected for a surface limited reaction.

2. A second shoulder E' appears on the left side of peak F. This shoulder is only just resolvable at 80 mV/sec.

3. Peak G has shifted almost 40 mV more negative. This would indicate that it is not the same type of peak as C and D, but may be an accidental maximum caused by the overlap of two more irreversible processes.

4. At this sweep speed the effects of Cl^- are detectable even at 50 r.p.m. and saturation with Cl^- is reached at 3200 r.p.m.

5. A limiting value of peak I is again reached at saturation , even though all shoulders before peak F' have been masked.

6. The Cl^- desorption plateau L is the same even in the presence of the oxygen reduction reaction except that it is displaced downward.

The situation with additions of $SO_4^=$ is not as well defined. A series of runs with additions to make the solution 1×10^{-7} to 1×10^{-4}M of $SO_4^=$ were done, including both rotation rate and window opening experiments. Figure 9 shows a selected few of these curves for a concentration of 3×10^{-6}M:

1. No clear isopotential points were observed as was the case for Cl^- additions.

2. The family of curves under rotation is quite different than those obtained for Cl^- adsorption. Thus, different adsorbing anions produce different effects.

3. A small peak appears between 250 to 300 mV which is clearly associated with the presence of $SO_4^=$.

4. The secondary oxide reduction peaks corresponding to I and J of Fig. 3b are similarly suppressed.

At low resolution, the anion desorption peak appears similar to Fig. 4. Figure 10 shows the double layer region at 10x sensitivity.

1. In the positive sweep, a small peak for the adsorption of Cl^- is seen at -30 mV.

2. The development of the $SO_4^=$ peak at 250 to 300 mV is clear.

3. Without rotation, two desorption peaks, one for Cl^- at 10mV and one for $SO_4^=$ at 220 mV are seen.

4. For higher rotation rates, the amount of Cl^- desorbed increases while the $SO_4^=$ peak shifts to more positive values, but does not appear to increase in size.

5. As the Cl^- desorption peak approaches saturation, the $SO_4^=$ desorption appears to merge with the Cl^- .

Figure 11 shows two curves for the < 100 > face in 0.1M HF at 20 mV/sec. A complete set was not run because of obviously high levels of Cl^- and $SO_4^=$ contamination visible in the double layer, but the two curves at 0 and 400 r.p.m. correspond very closely to those obtained for 0.01M $HClO_4$ at 400 and 1600 r.p.m. as shown in Fig. 3b with peaks C, D, and F still visible at 0 r.p.m. The only significant difference appears to be the vanishing of peak I at 400 r.p.m., which appears to be caused by $SO_4^=$. The concentration of this electrolyte was, however, ten times that of Fig. 3b.

< 111 > face

Figure 12a shows the set of curves for the < 111 > face for the same conditions as Fig. 3b. The inset (Fig. 12b) shows the double layer region only, taken at an expanded scale to show some of the details that are hidden by curve overlap. The overall shape of the curves is, as expected, different for this face, but the following significant differences and similarities are observed:

1. No changes in the curves with rotation were observed until 400 r.p.m., twice the rotation rate that was required for the < 100 > face. This could be caused by a lower anion level for that batch of electrolyte, or a smaller Q_{ads} since the potential at which Cl^- completely desorbs (and hence adsorbs, although the adsorption is diffusion limited and not as directly observable) is 240 mV more positive than for the < 100 > face.

2. The general effect of increasing rotation rate is the same in that all of the features (except A) before the isopotential point at 1020 mV are suppressed. The missing charge shows up in a new peak F which is not visible in the unrotated curve.

3. The satellite peaks I and J are not as well resolved as on the < 100 > face, but peak J clearly is being reduced at rotation rates 25 less than required for the decrease of peak I.

4. The anion desorption plateau again looks Temkin-like, but is more compressed by the end of I and J.

5. Saturation was not reached at 10,000 r.p.m. on this face (and this solution) even though the sweep rate was reduced to 20 mV/sec.

6. From the expanded d.l. curves (inset 12b) we can see that A grows to a limiting value while B is depressed. Peak A shows an anionic adsorption process, and is compressed towards positive values because of the higher potential for adsorption (240 mV compared to the < 100 > face).

7. The desorption of Cl^- at low rotation rates appears more peaked, looking like a lower r-value, but spreads out to the more Temkin-like shape at higher coverages.

Figure 13 shows curves for the < 111 > face in 0.1M *HF* at 0 and 200 r.p.m. at 20 mV/sec. Considerable $SO_4^=$ is present as can be seen from the peaks at 400–450 mV in the d.l. region (shown expanded as an inset). At 0 r.p.m. peaks E and F are still visible , while at 200 r.p.m. the surface appears saturated and only peak G is visible.

Voltammetry curves were also obtained for thin (1000 Å) films of *Au* that were epitaxially grown on cleaved mica by vapor deposition at a substrate temperature of 350° C. LEED showed a < 111 > orientation but with a very high background. ESCA showed a very clean surface with only traces of carbon from the chamber vacuum. SEM micrographs (Fig. 14) showed a fine grained oriented polycrystalline film with a profusion of grain boundaries, gaps and edges. These curves were taken before the study of the effects of impurities were begun. They are essentially the same as those taken for high quality massive single crystal < 111 > at rotation speeds of 200 r.p.m., including the humps in the double layer associated with anionic adsorption. It would appear that the use of such curves to characterize the condition of the surface may not be warranted.

< 110 > and < 331 > faces

Curves for selected rotation rates at 20 mV/sec for the < 110 > face and for the < 331 > faces are shown in Figs. 15 and 16. The effect of rotation on the behavior of these faces is so similar to those described above, including the appearance of the isopotential point and the way desorption of the anions occurs, that a detailed description of the figures is unnecessary.

DISCUSSION

It appears clear that the level of anionic impurities that are present even in electrolyte solutions prepared carefully from the purest commercially available sources is sufficient to alter the appearance of single crystal voltammetric curves. It is also clear that the causes of the discrepancies to be found in the literature (see Figs. 1 and 2) are more likely to be traces of anions than differences in surface preparation.

In all cases studied, the effects of Cl^- and $SO_4^=$ ion adsorption can be identified and resolved (with more or less difficulty). The shift of the peaks and the shape of the curves, in general, are directly dependent on the initial concentrations of impurity anions. The desorption of these anions occurs after the reduction process is completed. Both anions appear to stay on the surface during the entire oxide formation and reduction process, and it may be that $SO_4^=$ or HSO_4^- stays on the surface even during vigorous H_2 evolution. Bewick [22] has shown from EMIRS studies that there is IR evidence for $SO_4^=$ adsorbed on metal surfaces under these conditions. Occasionally, our crystals appeared contaminated with large quantities of $SO_4^=$ (identified from the shapes of the peaks in the double layer region, probably a result of accidental contamination) that disappeared only slowly on extended cycling (30–50 cycles) into the oxide and H_2 potentials. Since it is unlikely that the ions were destroyed (as are organics), and subsequent curves behaved "cleanly", it appears that the $SO_4^=$ (or more likely, the HSO_4^- ion) sticks tenaciously to the surface.

At low concentrations, where there is little overlap of the desorption peaks, the specific effects of the two anions are restricted to smaller potential ranges and can be differentiated from the behavior of the intrinsic double layer capacitance. It is clear that the potentials at which the anions

Table 1: SOME VALUES FOR THE FACES STUDIED*

Crystal Face	PZC [28] 0.01 M NaF	PZC [11] 0.099M $NaClO_4$ +0.001M $HClO_4$	End of Cl^- Desorption	Start of Desorption	Isopotential Point
< 111 >	+320	+240**	+170 to 180	+250 to 260	1020
< 110 >	-60	-20	-100	+50	1090
< 100 >	+100	+80**	-70 to -40	+75 to +85	1045
< 331 >	-50	—	-100 to -150	(broad)	1040

* Potentials reported as mV *vs.* SCE.
** Measured in unspecified "more dilute solution".

(in particular the Cl^- ion) desorb are different for each crystal face studied (see Table 1). Since the small peaks that are almost universally to be seen in the double layer region of the reported curves had not previously been positively identified with impurity anions, it is understandable that they have been associated with specific adsorption of ClO_4^- [9,22] and F^- ions [13,24]. It has been the experience of this laboratory from capacity measurements on polycrystalline *Au* [25] that in rigorously cleaned and preelectrolyzed solutions where strict attention has been paid to maintaining a symmetric geometry (to minimize frequency dispersion caused by non-uniform current distribution [25]), the phase angle for capacitance measurements in the double layer region is within experimental limits an ideal $-90°$. When a specifically adsorbed anion is present, the double layer must be represented with an additional series RC term in parallel [21], where the R is the adsorption reaction resistance for the pseudo-capacitance C. If this additional RC term is not accounted for, it will appear as an artifactual frequency dispersion term in the value calculated for the C_{dl}. Taken together with the distribution of desorption resistances to be found with a Temkin-like isotherm, this "RC" term will appear as a "constant phase element" (CPE) as described by Sluyters *et. al.* [8,27].

It is probably no coincidence that the reported values for the PZC [11,28,29] lie close to the minimum in the CV curves (and hence capacity) in the potential region below the $SO_4^=$ desorption peak and above that for Cl^-. We have seen that the potentials at which these anions desorb are strongly dependent on the crystal face in the sequence predicted from the variation of the work function. The capacitance measured at potentials more negative than that at which Cl^- desorbs is significantly smaller than those reported for the PZC. Keeping in mind the presence of ionic impurities for which:

1. concentration will be a function of the composition of the electrolyte,
2. surface concentration will be a function of the anodic sweep limit,
3. diffusion will be controlled by the temperature, it becomes clear why so many puzzling properties and variabilities of the "PZC" have been reported [30].

Although more difficult to quantify, it was generally observed while running the experiments described above that the ease of getting a "clean" set of curves was in the order < 111 > - < 100 > - < 110 >. This is the order in which the desorption of anions is to be found on the several surfaces.

The "cleanest" behavior should be observed on the surface which has the narrowest window for anion adsorption, i.e. the potential region between the onset of adsorption and the onset of oxide formation. This appears to be the case, for example, for the rotation rate at which anion saturation occurred, and for anion effects on the H_2 evolution reaction [31]. Tafel plots for this reaction on the < 111 > face had linear slopes of $\approx$ 90 mV/dec. over 4 to 5 decades when cycled between -800 mV and 0V SCE. On the < 100 > face, a straight line was only obtained when the electrode was cycled above +800 mV, while the < 110 > face was still slightly curved even when cycling to 1400 mV. On all faces the apparent exchange current decreased linearly with the square root of rotation rate, from which we can infer that some diffusion limited species is affecting the reaction.

While this study has been restricted primarily to surfaces of single crystals of gold, preliminary studies on polycrystalline *Au*, single and poly-crystal *Pt* and on other metals show that similar effects are induced by rotation. Until this question has been satisfactorily resolved, it is difficult to establish which parts of the single crystal literature are valid and which parts are open to serious questions of purity.

CONCLUSIONS

1. The purest commercially available $HClO_4$ and HF have sufficient residual Cl^- and $SO_4^=$ to affect the shape and/or appearance of single crystal C.V. curves.

2. Most of the differences in these C.V. curves reported in the literature can be quantitatively reproduced by various combinations of rotation rate and/or intentional impurity additions.

3. The analysis of the effects of Cl^- addition is more straightforward than for $SO_4^=$ additions. The later interacts with the surface more strongly than the former.

4. Cycling into the oxide region appears to remove cationic impurities and possibly organic contaminants, but not Cl^- and $SO_4^=$. Both anions apparently remain on the surface even during the formation of the first complete monolayer of oxide. The anions may be chemically incorporated into the initial layer.

5. Evidence presented in the literature as evidence for the specific adsorption of ClO_4^- and F^- ions is probably better interpreted as having been caused by unsuspected traces of low levels of impurities in the electrolyte.

6. Cycling into the H_2 region removes Cl^- but HSO_4^- or $SO_4^=$ may remain even during vigorous H_2 evolution. Cationic impurities can adsorb during this potential excursion, however.

7. Low level impurity effects are a possible cause for the apparent curvature and other anomalies reported for Tafel slopes for H_2 evolution on single crystal *Au*.

8. Cl^- and $SO_4^=$ adsorption on single crystal surfaces is in the order 110 > 100 >> 111. This is the same sequence expected on the basis of theoretical arguments based on work function measurements , but the reported values for the PZC may be in error. The reported capacitance minimum values appear to coincide with the potential at which $SO_4^=$ finishes desorbing and Cl^- begins.

9. The "constant phase angle" reported for *Au* capacitance measurements in the region of the apparent PZC may be caused by the RC term for the pseudo-capacitive adsorption-desorption reaction in parallel with the double layer capacitance. The capacitance of the *Au* interface is 50–100% lower at potentials significantly below the reported PZC and has a phase shift very close to $-90°$.

10. The "fingerprint" concept is more clearly a justifiable criterion for assessing the purity of electrolyte than the perfection of the crystal.

11. No electrochemical evidence of "restructuring" of the gold surface was detected on cycling between H_2 evolution potentials and 1400 mV (SCE) at which point a complete monolayer has been formed. Higher potentials (and multilayer formation) may produce such effects.

12. Discrepancies in the literature for other single crystal materials may also be at least partially due to residual impurities.

REFERENCES

1. A. D'Agostino and P. N. Ross, J. Electroanal. Chem., **189**, 371 (1985).

2. J. Lecoeur, C. Sella, L. Tertian, and A. Hamelin, C. R. Acad. Sci. Paris, **280** Serie C, 249 (1975).

3. A. Hamelin, J. Electroanal. Chem., **195**, 175 (1985).

4. D. Dickertmann, J. W. Schultze and K. J. Vetter, J. Electroanal. Chem., **55**, 429 (1974).

5. D. M. Kolb and J. Schneider, Electrochim. Acta, **31**, 929 (1986).

6. A. Hamelin and S. Rottgermann, Electrochim. Acta, **32**, 723 (1987).

7. A. T. D'Agostino and P. N. Ross, Surf. Sci., **185**, 88 (1987).

8. G. Brug, M. Sluyters-Reybach, J. Sluyters and A. Hamelin, J. Electroanal. Chem., **181**, 245 (1984).

9. H. Angerstein-Kozlowska, B. Conway, A. Hamelin and L. Stoicoviciu, Electrochim. Acta, **31**, 1051 (1986).

10. C. Pedriel, A. Arvia and M. Ipohorski, J. Electroanal. Chem., **215**, 317 (1986).

11. A. Hamelin and M. J. Weaver, J. Electroanal. Chem., **223**, 171 (1987).

12. A. Hamelin, J. Electroanal. Chem., **210**, 303 (1986).

13. A. Hamelin, J. Electroanal. Chem., **138**, 395 (1982).

14. J. D. E. McIntyre and W. F. Peck, Jr., J. Electrochem. Soc., **123**, 1800 (1976).

15. R. R. Adzic and N. M. Markovic, J. Electroanal. Chem., **138**, 443 (1982).

16. B. D. Cahan and H. M. Villullas, submitted for publication.

17. D. M. Zehner, private communication.

18. K. Engelsmann, W. Lorentz and E. Schmidt, J. Electroanal. Chem., **114**, 1 (1980).

19. B. D. Cahan and H. Song, to be published.

20. D. Dickertmann, F. D. Koppitz and J. W. Schultze, Electrochim. Acta, **21**, 967 (1976).

21. E. Gileadi, E. Kirowa-Eisner, J. Penciner, Interfacial Electrochemistry, Addison-Wesley (1975).

22. A. Bewick and R. J. Nichols, ECS Meeting, Atlanta (1988).

23. H. Angerstein-Kozlowska, B. E. Conway, A. Hamelin and L. Stoicoviciu, J. Electroanal. Chem., **228**, 429 (1987).

24. A. Hamelin and A. Le Lan, C. R. Acad. Sci. Paris, Ser. II, **295**, 161 (1982).

25. B. D. Cahan and C. T. Chen, J. Electrochem. Soc., **129**, 700 (1982).

26. B. D. Cahan and H. Song, Toronto Meeting ACS (1988).

27. G. J. Brug, A. L. G. Van den Eeden, M. Sluyters-Reybach and J. H. Sluyters, J. Electroanal. Chem., **176**, 275 (1984).

28. J. Lecoeur, J. Andro and R. Parsons, Surf. Sci., **114**, 320 (1982).

29. A. Hamelin, T. Vitanov, E. Sevastianov and A. Popov, J. Electroanal. Chem., **145**, 225 (1983).

30. A. Hamelin in Modern Aspects of Electrochemistry, Vol. 16, Plenum Press, New York (1986).

31. B. D. Cahan, H. M. Villullas and E. Yeager, in preparation.

ACKNOWLEDGMENTS

This research has been supported by the Office of Naval Research and the Dept. of Energy.

LEGENDS FOR FIGURES

- Fig. 1.- Voltammetric curves for $Au < 111 >$ electrodes in different electrolytes taken from the literature (with permission from the publishers). a) A. T. D'Agostino and P. N. Ross, from reference [1]. b) J. Lecoeur, C. Sella, L. Tertian and A. Hamelin, from ref. [2]. c) A. Hamelin, from ref.[3]. d) After D. Dickertmann, J. W. Schultze and K. J. Vetter, from ref. [4]. e) After D. M. Kolb and J. Schneider, from ref [5].

- Fig. 2.- Voltammetric curves for $Au < 100 >$ electrodes in $HClO_4$ solutions taken from the literature (with permission from the publishers). a) After D. Dickertmann, J. W. Schultze and K. J. Vetter, from ref. [4]. b) After D. M. Kolb and J. Schneider, from ref [5]. c) A. Hamelin and S. Rottgermann, from ref. [6], d) A. T. D'Agostino and P. Ross, from ref. [7].

- Fig. 3.- a) C.V. curve for $Au < 100 >$ in 0.01 M $HClO_4$ at 80mV/s. The curve was obtained using IR compensation and correction. b) C.V. curves for $Au < 100 >$ in 0.01 M $HClO_4$ at different rotation rates (r.p.m.):(———) 0, (– – – –) 200, (– · · – · · –) 800,(· · · · · ·) 3200, (· – – · – – ·) 10,000. Sweep rate: 80 mV/s.

- Fig. 4.- C.V. curves for $Au < 100 >$ in 0.01 M $HClO_4$+2.5 x 10^{-6}M HCl at different rotation rates (r.p.m.): (———) 0, (– – – –) 200, (– · · – · · –) 800, (· · · · · ·) 3200, (· – – · – – ·) 10,000. Sweep rate: 80 mV/s.

- Fig. 5.- C.V. curves from window opening experiments in the double layer region for $Au < 100 >$ in 0.01 M $HClO_4$ at 0 and 10,000 r.p.m. Sweep rate: 80 mV/s. The dashed curves show the profile after entering into the oxide region.

- Fig. 6.- a) Desorption charge of anions (integrated from Fig. 3b) as a function of the square root of rotation speed. b) integrated charge differences (from Fig. 3b, see text) (1) for the oxide formed up to the isopotential point and (2) for the oxide reduced in the secondary peaks I and J as a function of the square root of rotation speed. c) integrated charge difference for the oxide formed up to the isopotential point as a function of the desorption charge of anions.

- Fig. 7.- a) Desorption charge of Cl^- (integrated from Fig. 4) as a function of the square root of rotation speed. b) Integrated charge difference (from Fig. 4) for the oxide formed up to the isopotential point as a function of the square root of rotation rate. c) Integrated charge difference for the oxide formed up to the isopotential point as a function of the desorption charge of Cl^- .

- Fig. 8.- C.V. curves for $Au < 100 >$ in 0.01 M $HClO_4$ at different rotation rates (r.p.m.): (———) 0, (– – – –) 200, (– · · – · · –) 800, (· · · · · ·) 3200, (· – – · – – ·) 10,000. Sweep rate: 20 mV/s.

- Fig. 9.- C.V. curves for $Au < 100 >$ in 0.01 M $HClO_4$+3 x $10^{-6}M$ H_2SO_4 at different rotation rates (r.p.m.): (———) 0, (– – – –) 200, (– · · – · · –) 800, (· · · · · ·) 3200, (· – – · – – ·) 10,000. Sweep rate: 80 mV/s. Curves were taken using IR correction and compensation.

- Fig. 10.- Expanded C.V. curves in the double layer region for $Au < 100 >$ in 0.01 M $HClO_4$+ 3 x 10^{-6}M H_2SO_4 at different rotation rates (r.p.m.): (———) 0, (– – – –) 200, (– · · – · · –) 800, (· · · · · ·) 3200, (· – – · – – ·) 10,000. Sweep rate: 80 mV/s. Curves were taken using IR correction and compensation.

- Fig. 11.- C.V. curves for $Au < 100 >$ in 0.1 M HF at 20 mV/s. at two rotation rates: (———) 0, (– – – –) 450,

- Fig. 12.- C.V. curves for $Au < 111 >$ in 0.01 M $HClO_4$ at different rotation rates (r.p.m.): (———) 0, (– – – –) 200, (– · · – · · –) 800, (· · · · · ·) 3200, (· – – · – – ·) 10,000. Sweep rate: 80 mV/s. b) Expanded curves in the double layer region.

- Fig. 13.- C.V. curves for $Au < 111 >$ in 0.1 M HF at 20 mV/s. The insert shows the expanded curve for the double layer region for rotation rates of (———) 0, (· · · · · ·) 50, (– – – –) 200,

- Fig. 14.- S.E.M. photographs of *Au* films grown by vapor deposition onto cleaved mica.
- Fig. 15.- C.V. curves for *Au* < 110 > in 0.01 M $HClO_4$ at different rotation rates (r.p.m.): (————) 0, (– – – –) 200, (– · · – · · –) 800, (· · · · · ·) 3200, (· – – · – – ·) 10,000. Sweep rate: 20 mV/s.
- Fig. 16.- C.V. curves for *Au* < 331 > in 0.1 M $HClO_4$ at different rotation rates (r.p.m.): (————) 0, (– – – –) 200, (– · · – · · –) 800, (· · · · · ·) 3200, (· – – · – – ·) 10,000. Sweep rate: 20 mV/s.

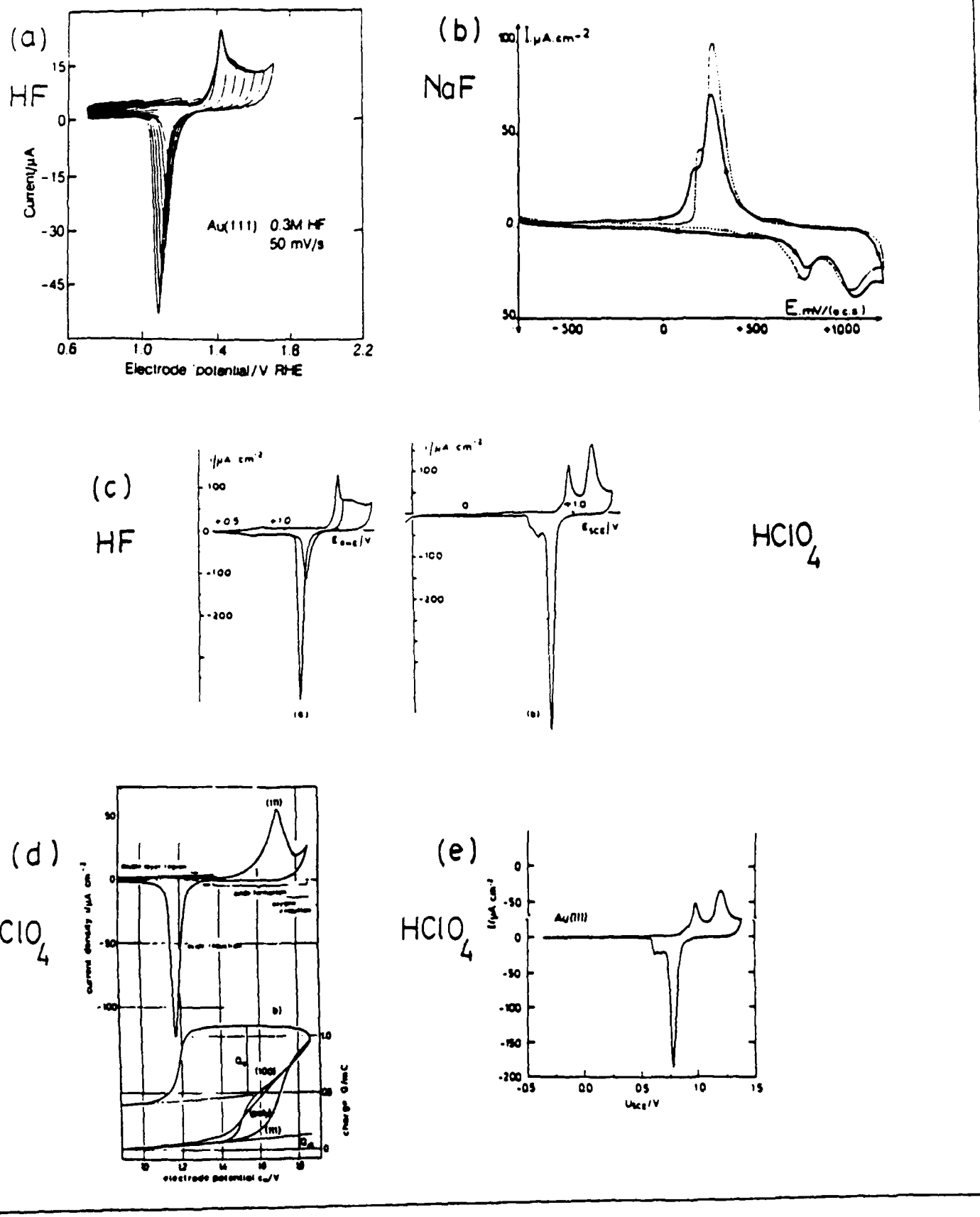
(a)
HF
Current/μA
Au(111) 0.3M HF
50 mV/s
Electrode potential/V RHE
(b)
NaF
E, mV/(s.c.e.)
(c)
HF
HClO4
(d)
HClO4
(e)
HClO4
Au(111)

Fig. 1.

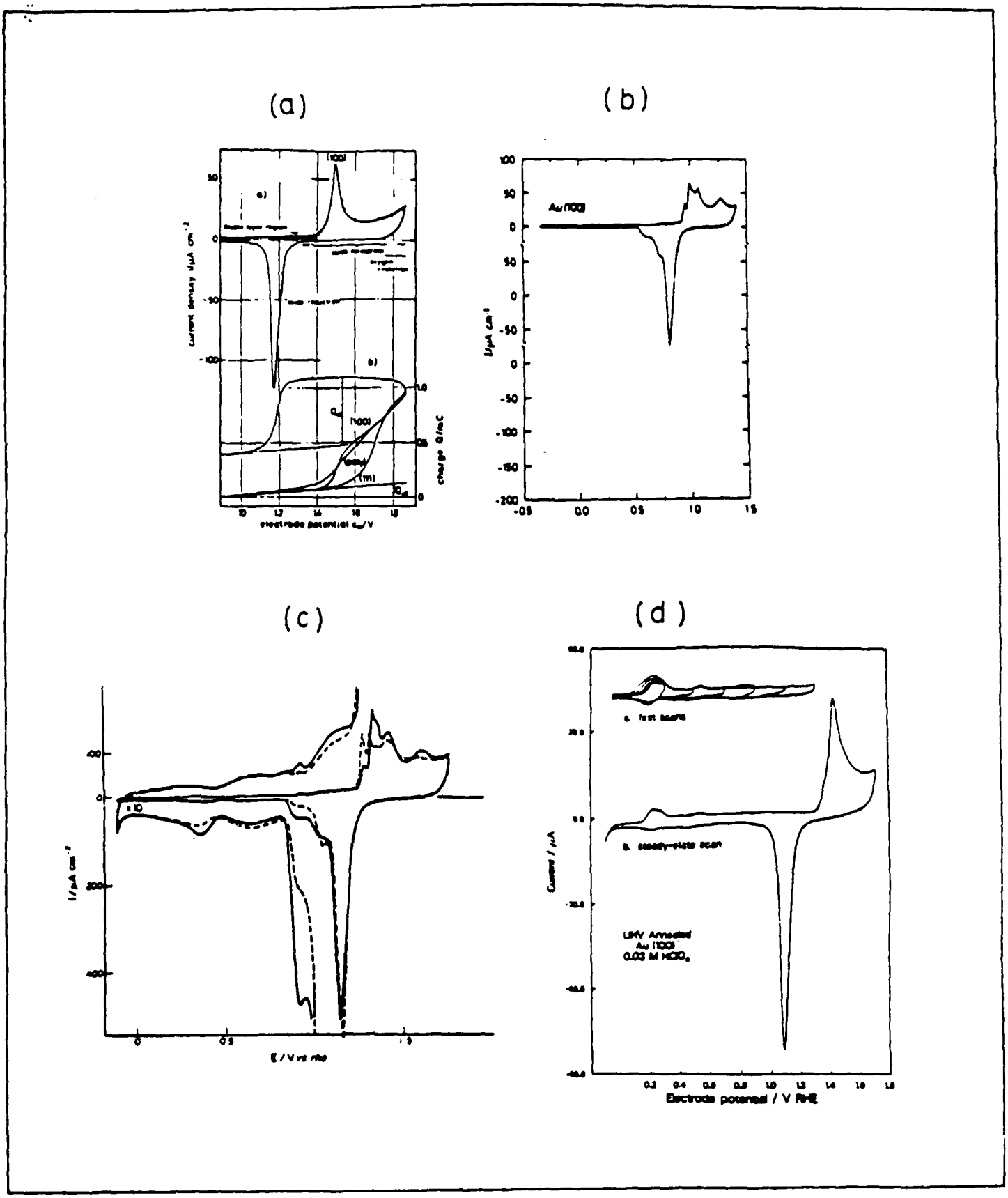
(a)
(b)
(c)
(d)
(100)
Au(100)
UHV Annealed
Au (100)
0.05 M HClO4
Electrode potential / V RHE

Fig. 2.

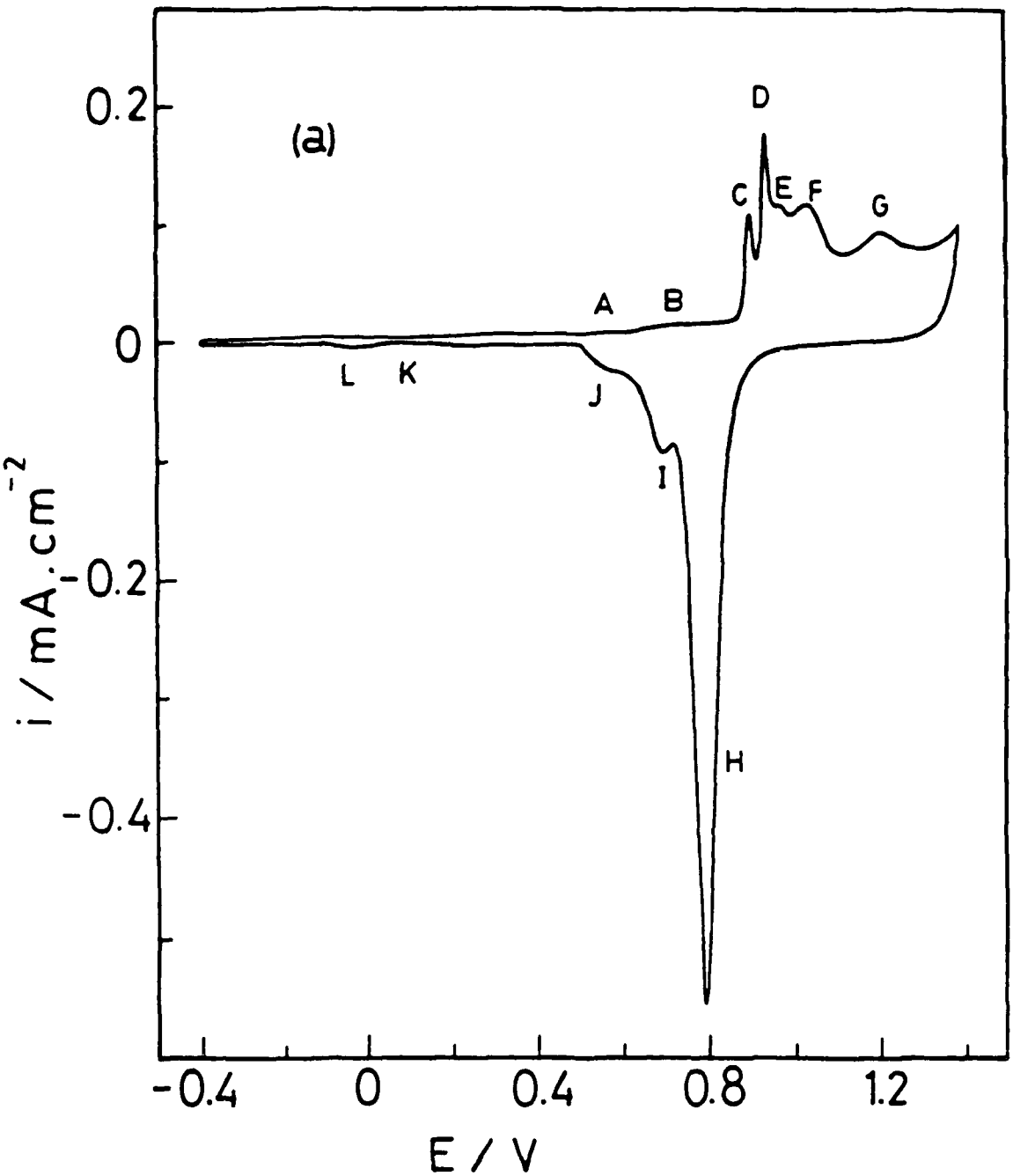

Fig. 3a.

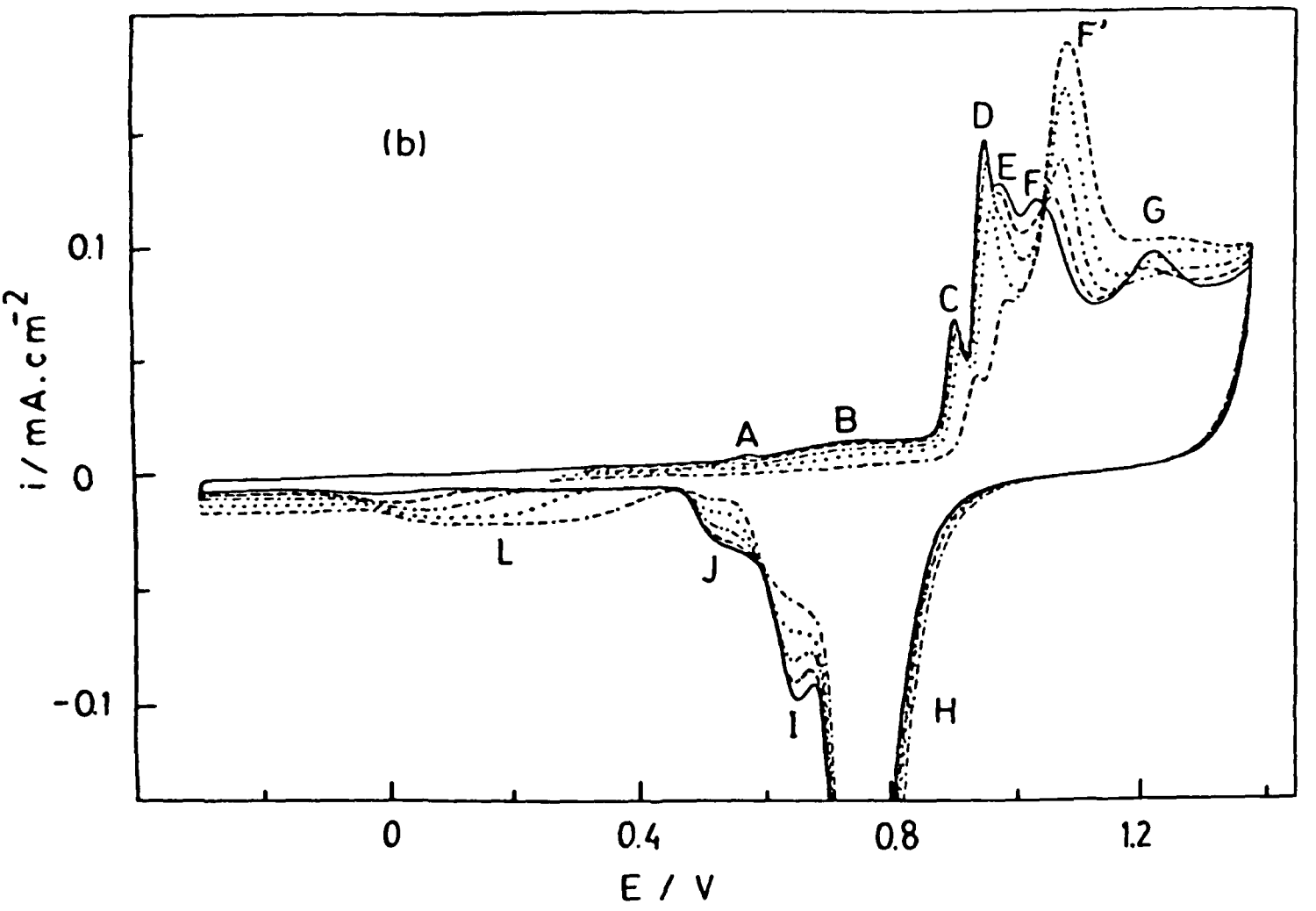

Fig. 3b.

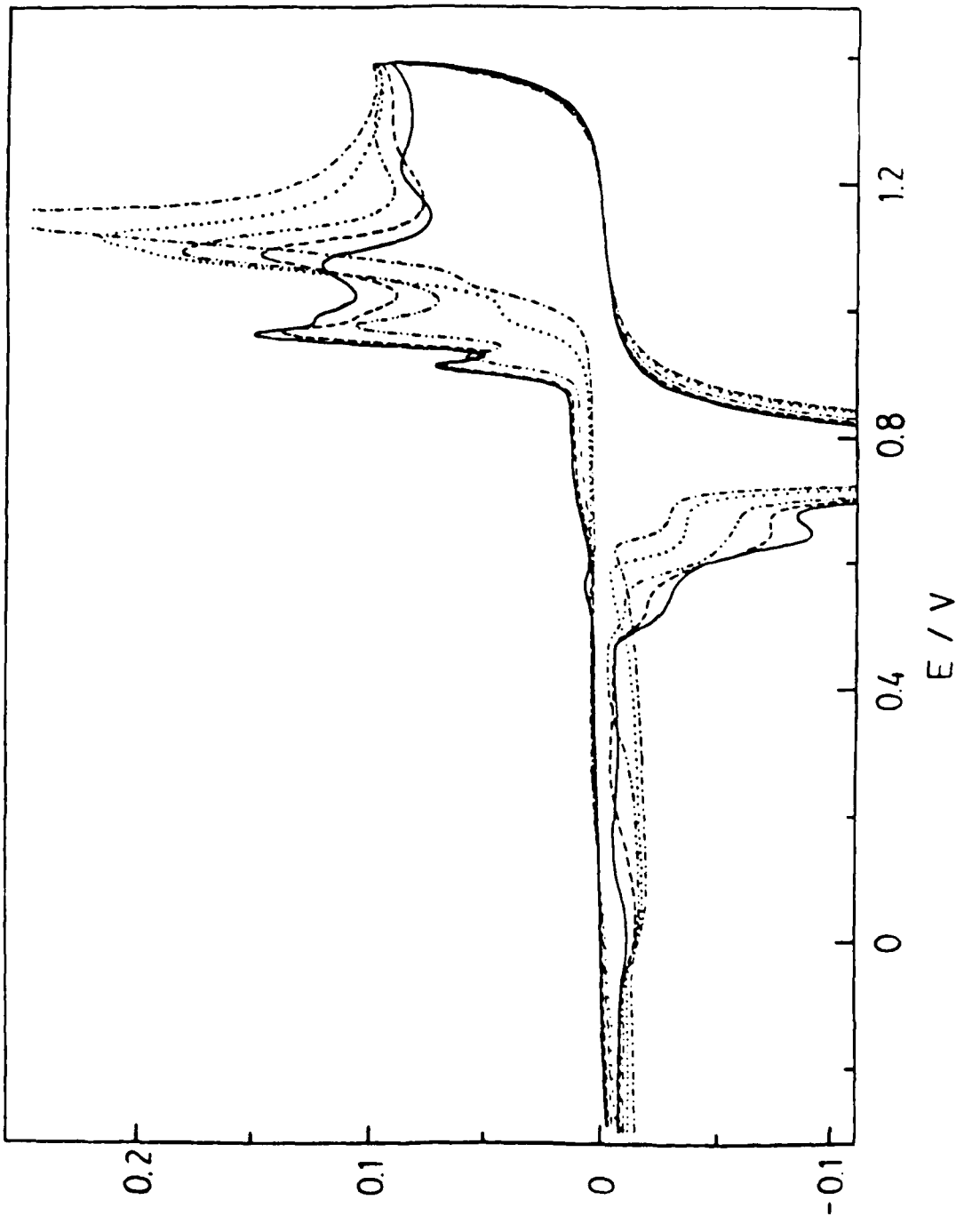

Fig. 4.

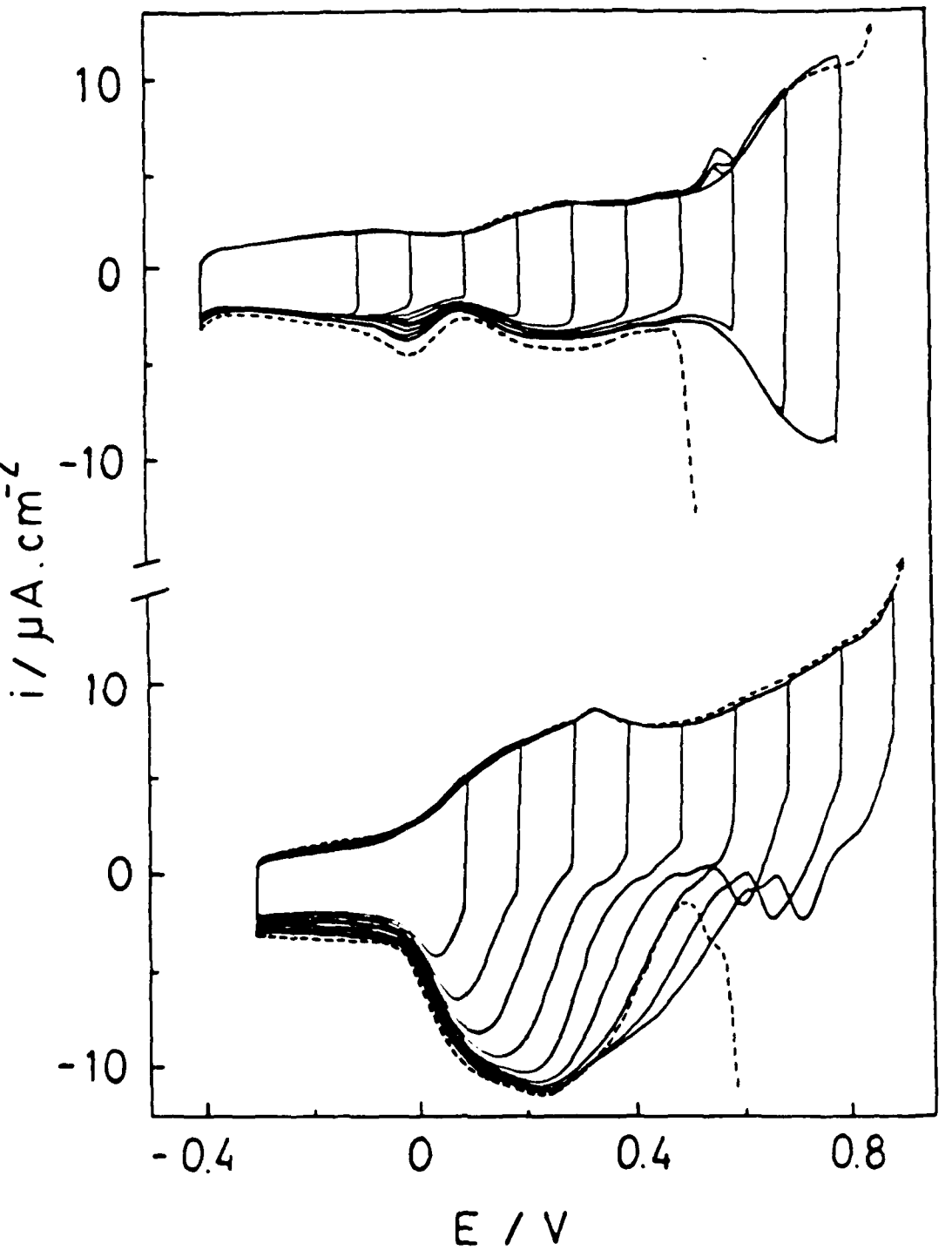

Fig. 5.

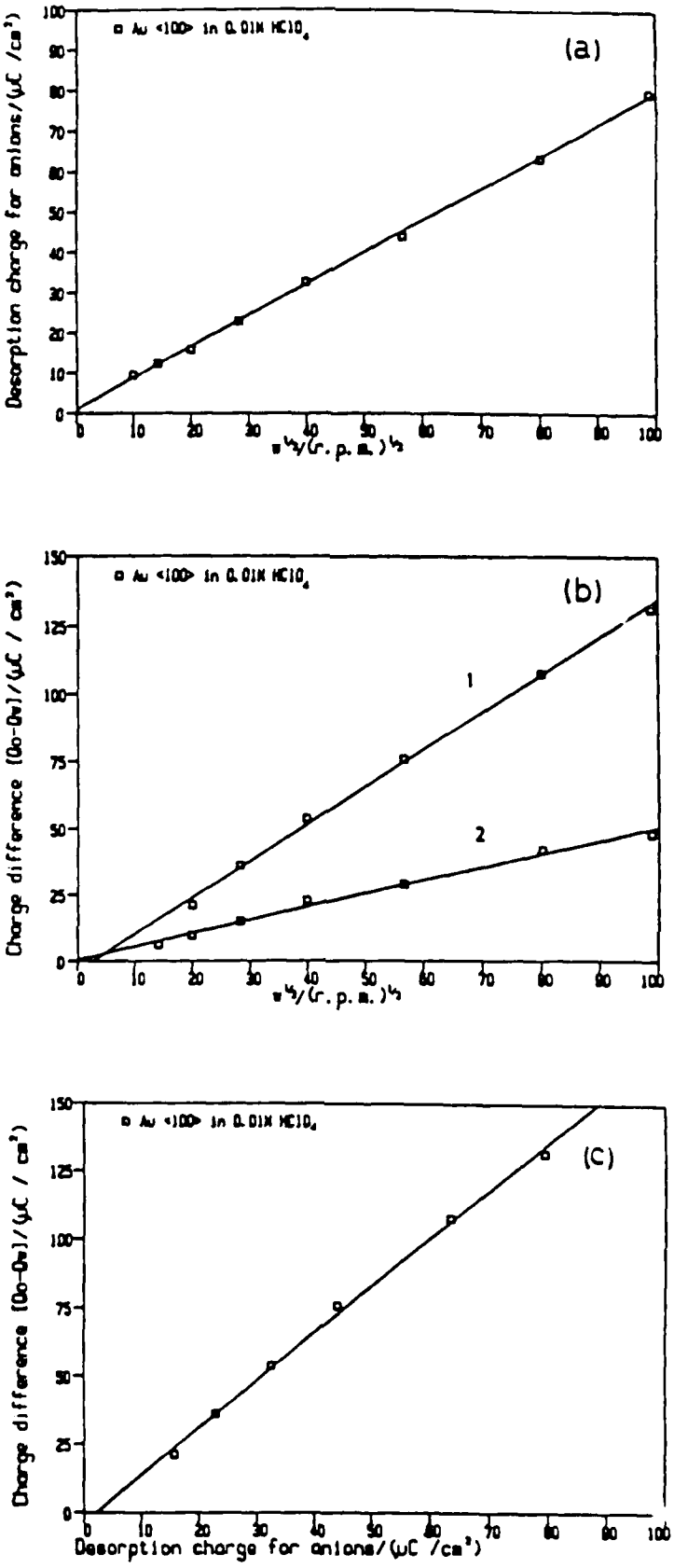
Au <100> in 0.01N HClO4
(a)
Desorption charge for anions/(μC /cm²)
w½/(r. p. m.)½
(b)
Charge difference (Qo-Qw)/(μC / cm²)
1
2
(c)
Desorption charge for anions/(μC /cm²)

Fig. 6.

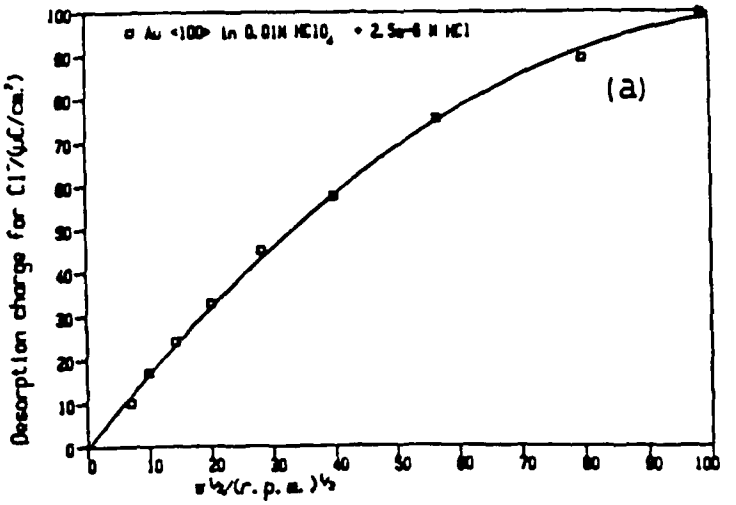
□ Au <100> in 0.01N HClO4 • 2.5e-6 N HCl
(a)
Desorption charge for Cl⁻/(μC/cm²)
ω^½/(r.p.m.)^½

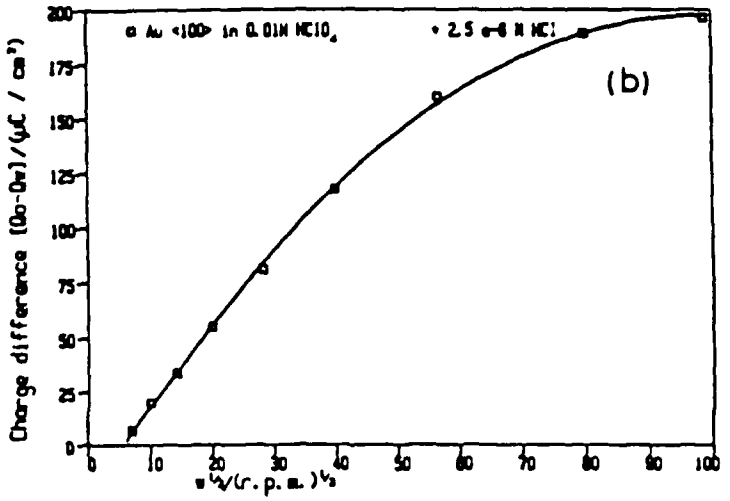
□ Au <100> in 0.01N HClO4 • 2.5 e-6 N HCl
(b)
Charge difference (Qo-Qw)/(μC / cm²)
ω^½/(r.p.m.)^½

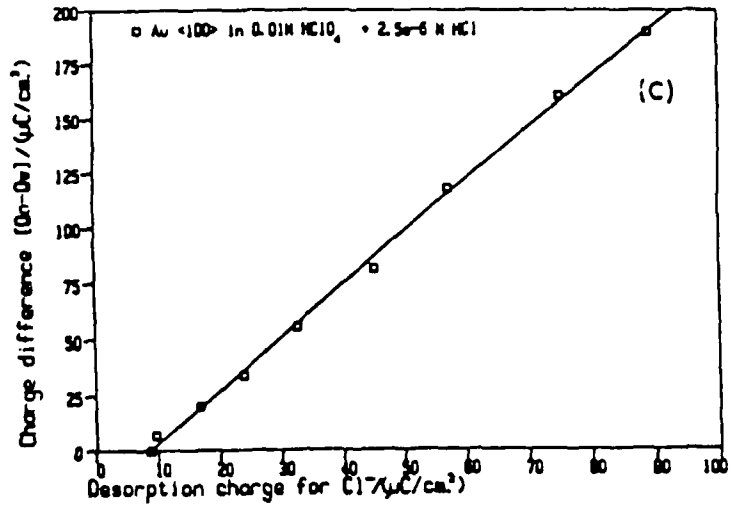
□ Au <100> in 0.01N HClO4 • 2.5e-6 N HCl
(c)
Charge difference (Qo-Qw)/(μC/cm²)
Desorption charge for Cl⁻/(μC/cm²)

Fig. 7.

Fig. 8.

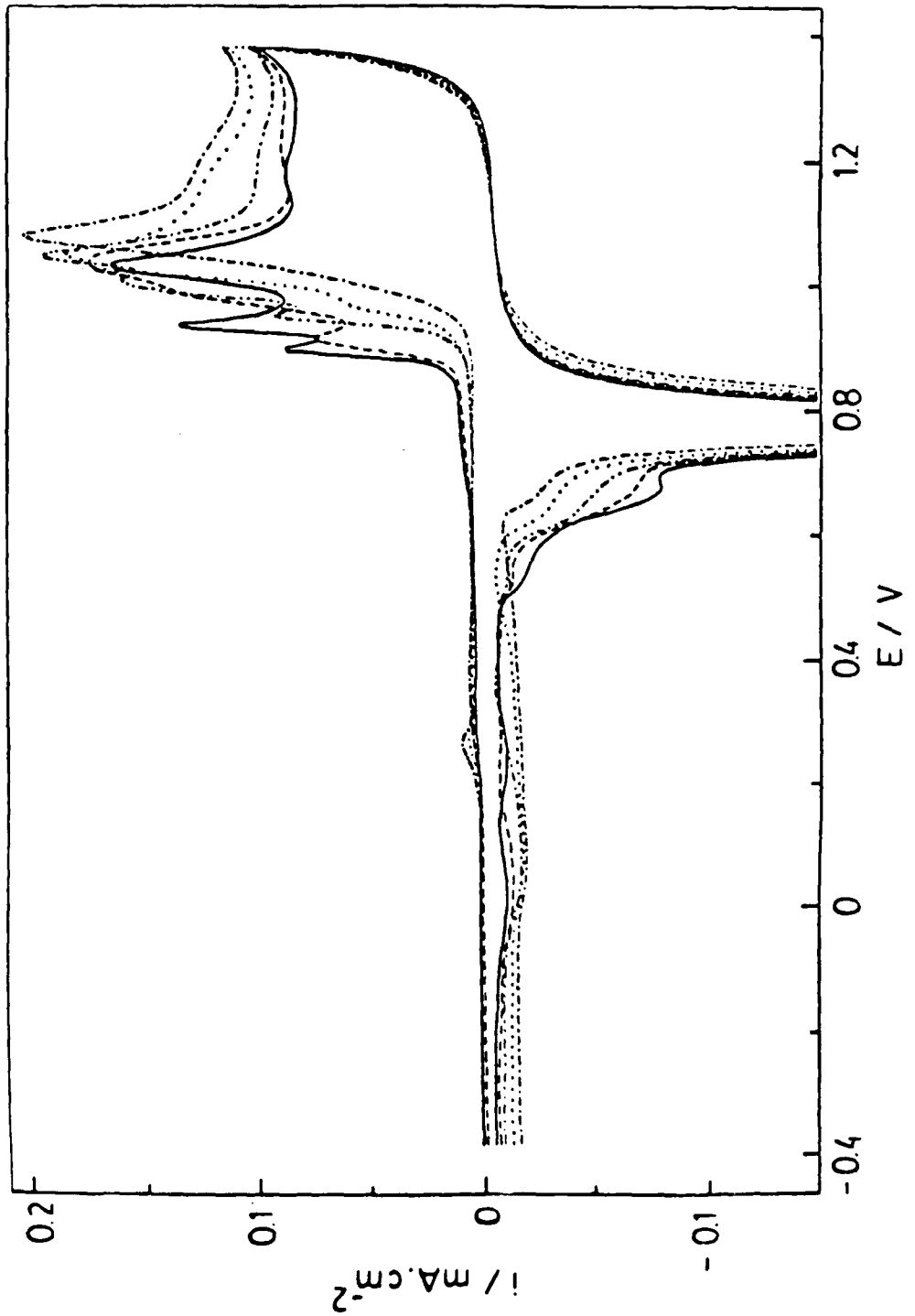

Fig. 9.

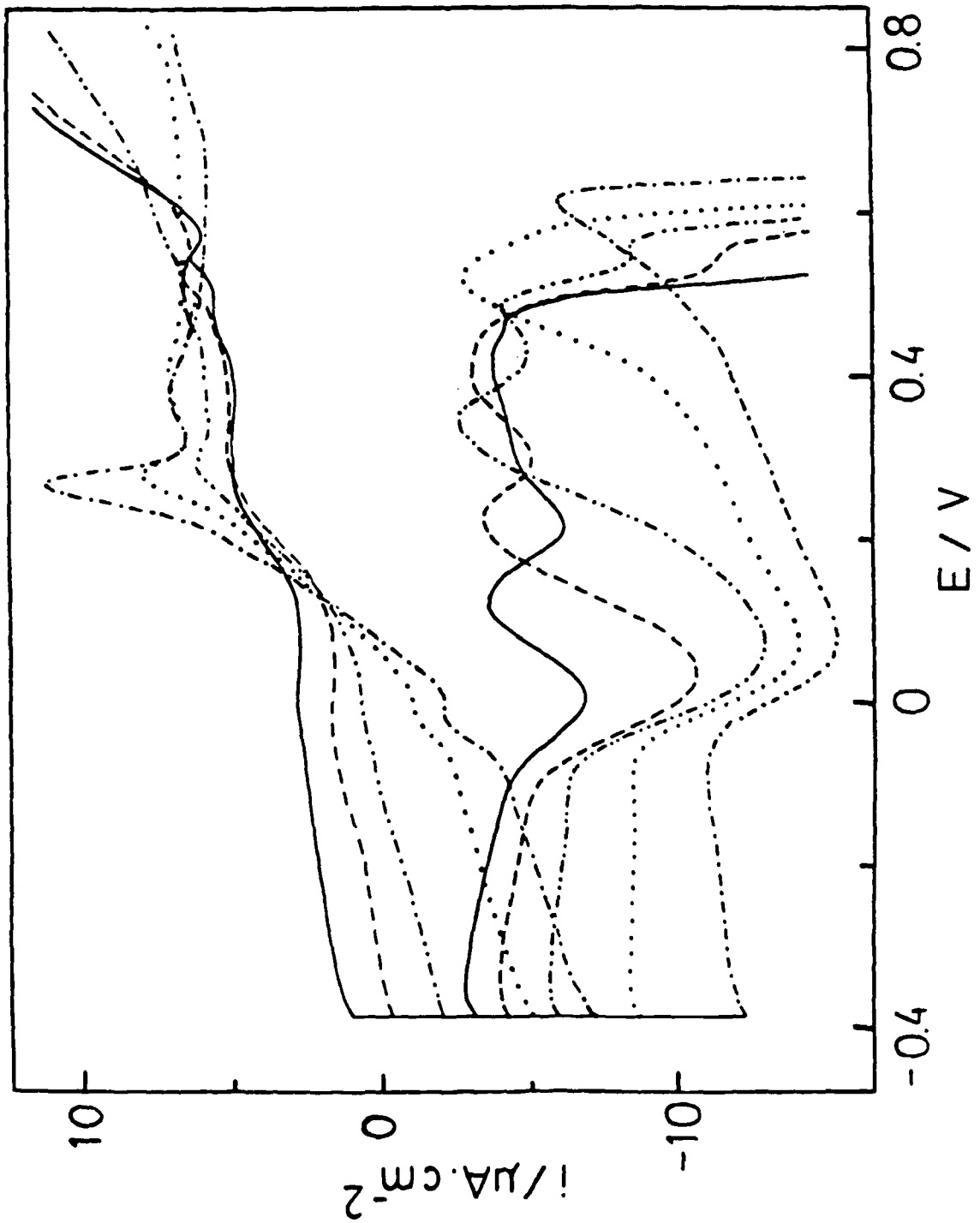

Fig. 10.

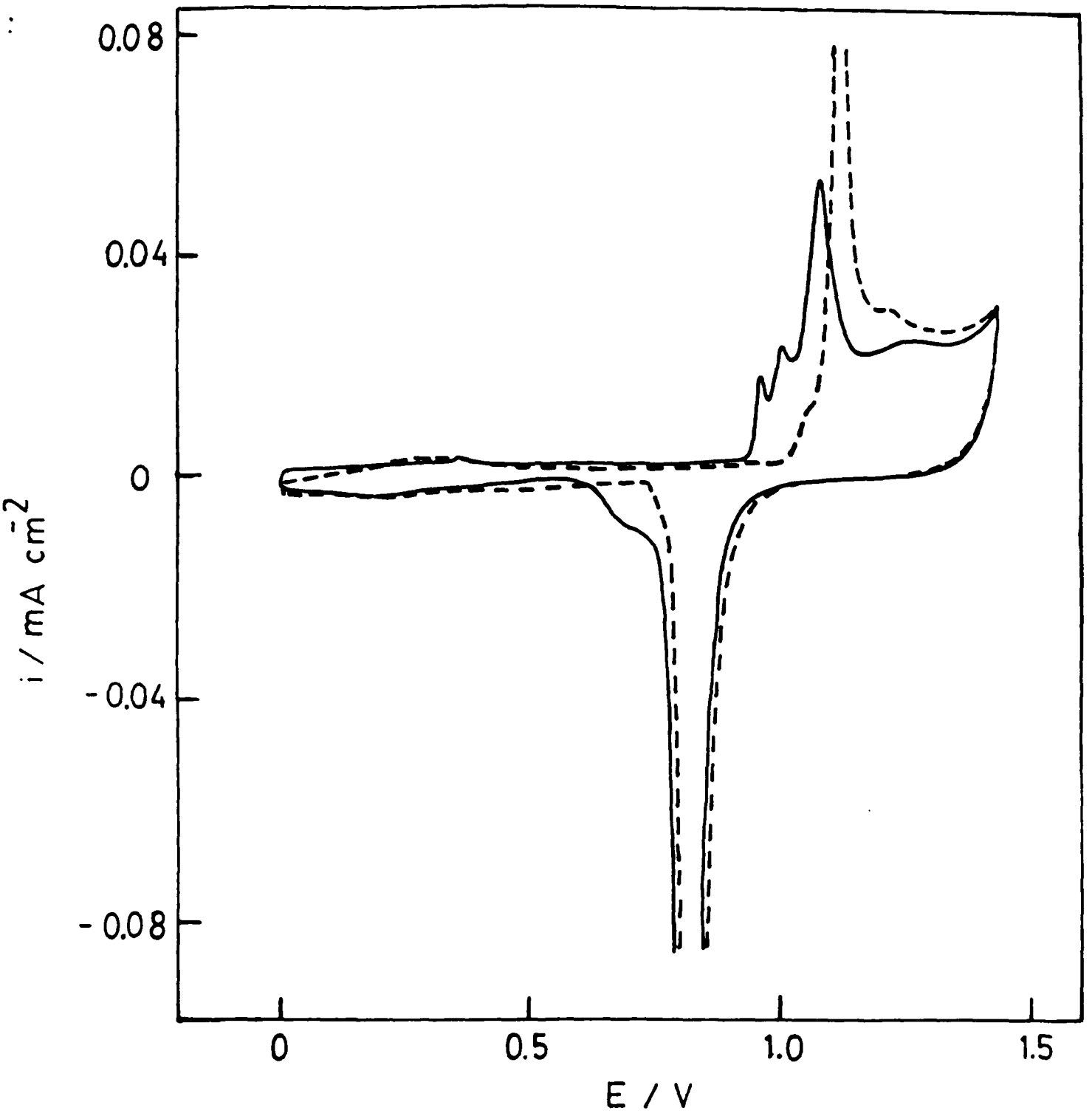

Fig. 11.

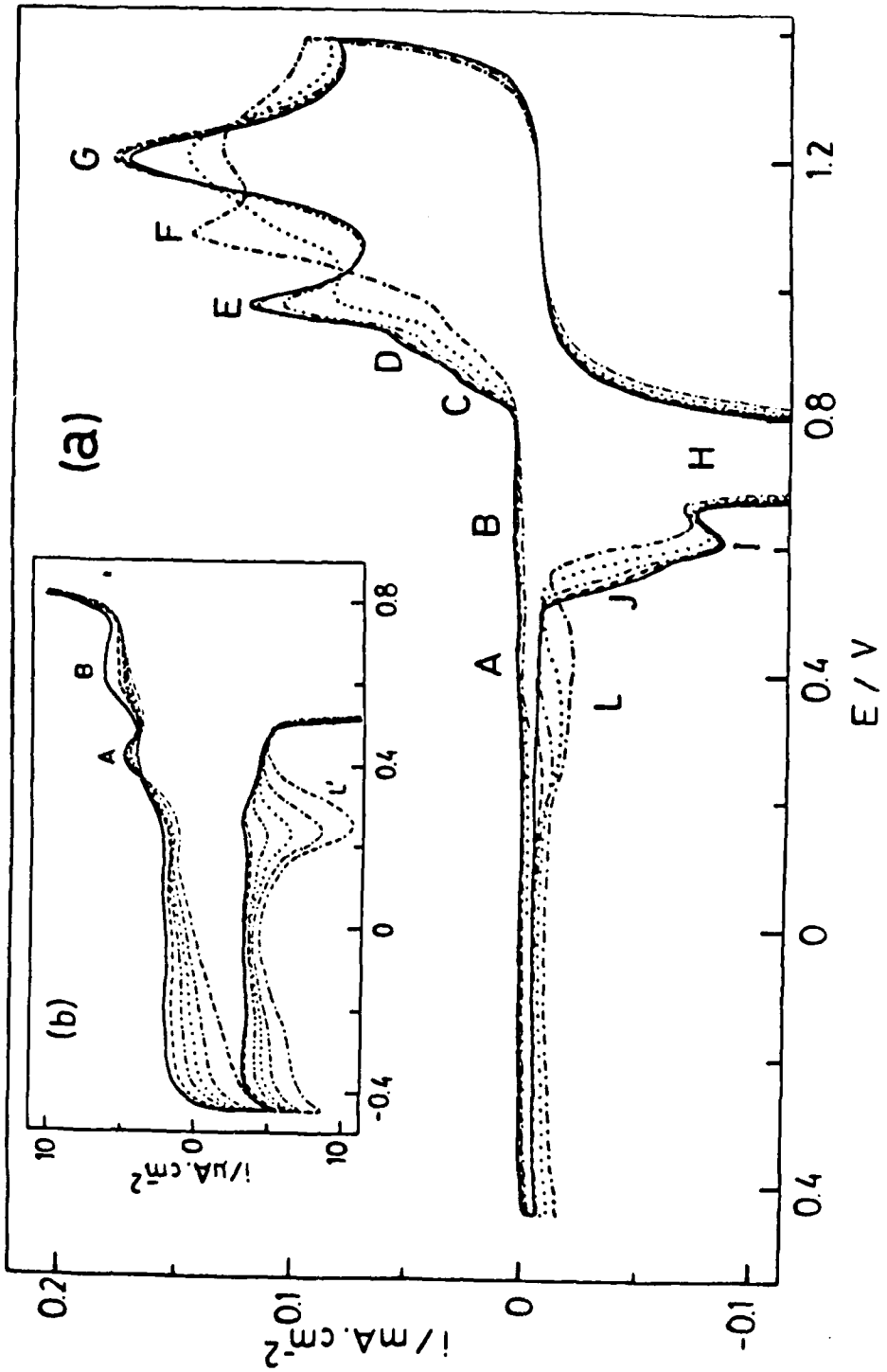

Fig. 12

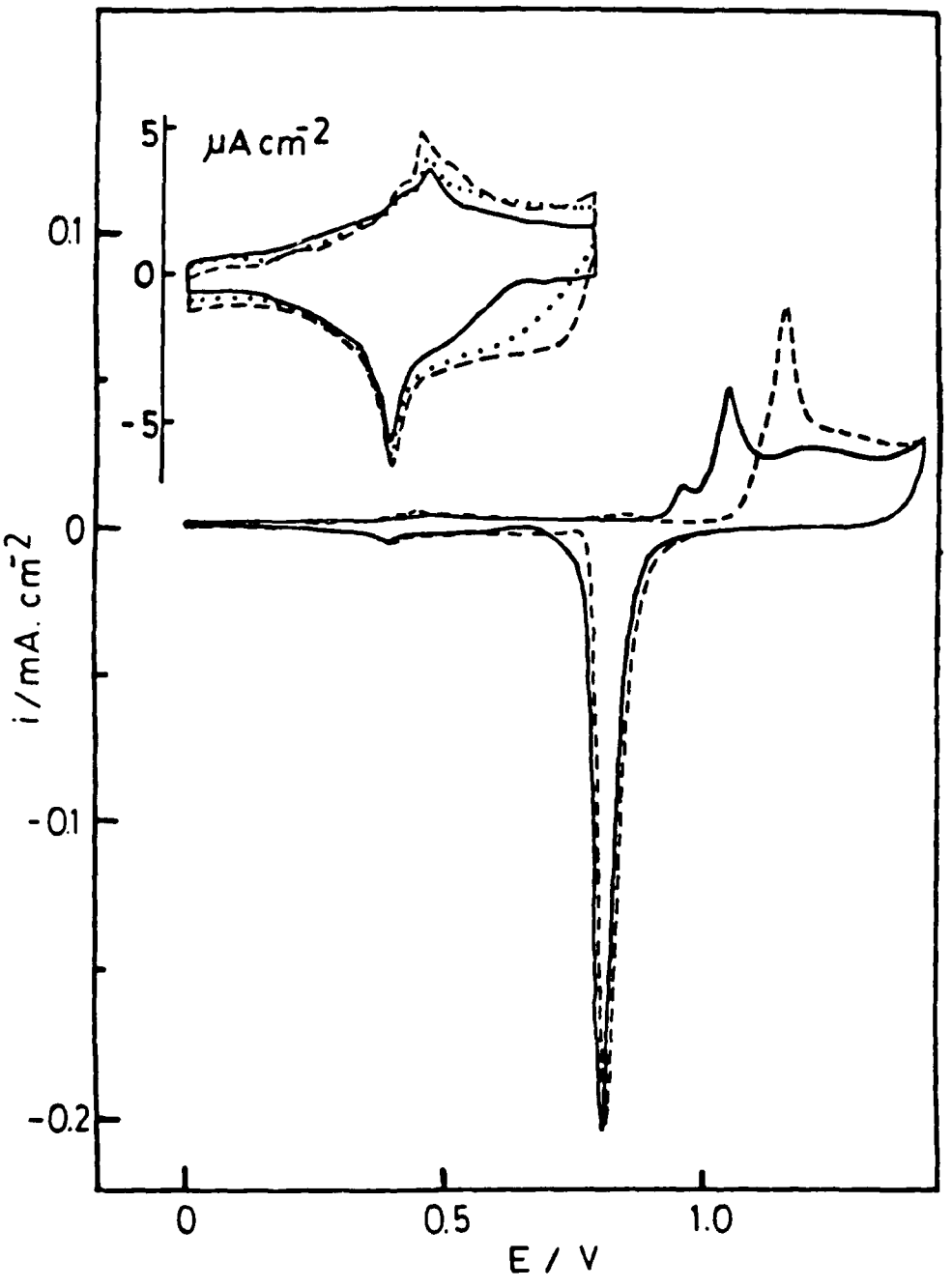

Fig. 13.

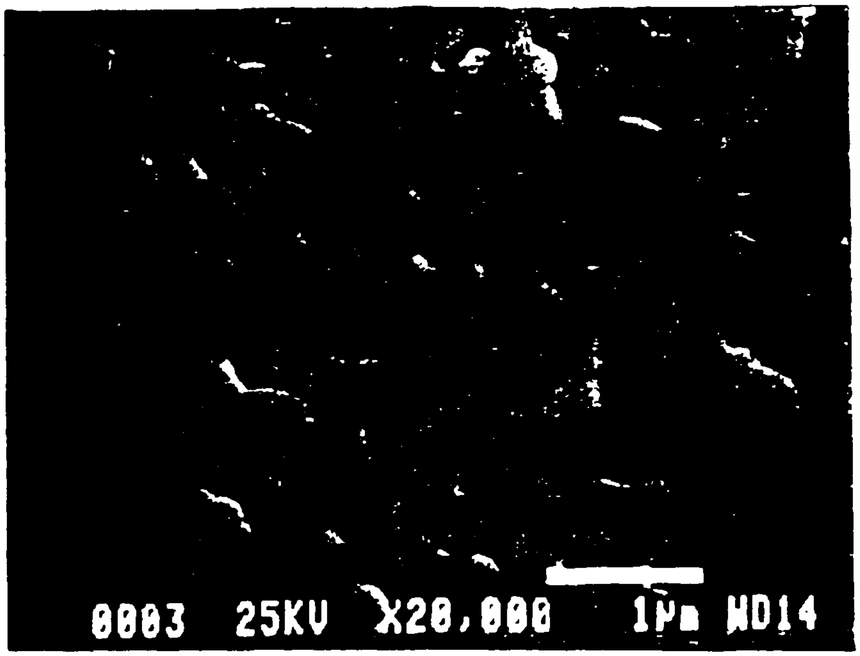
0003 25KV X20,000 1μm WD14

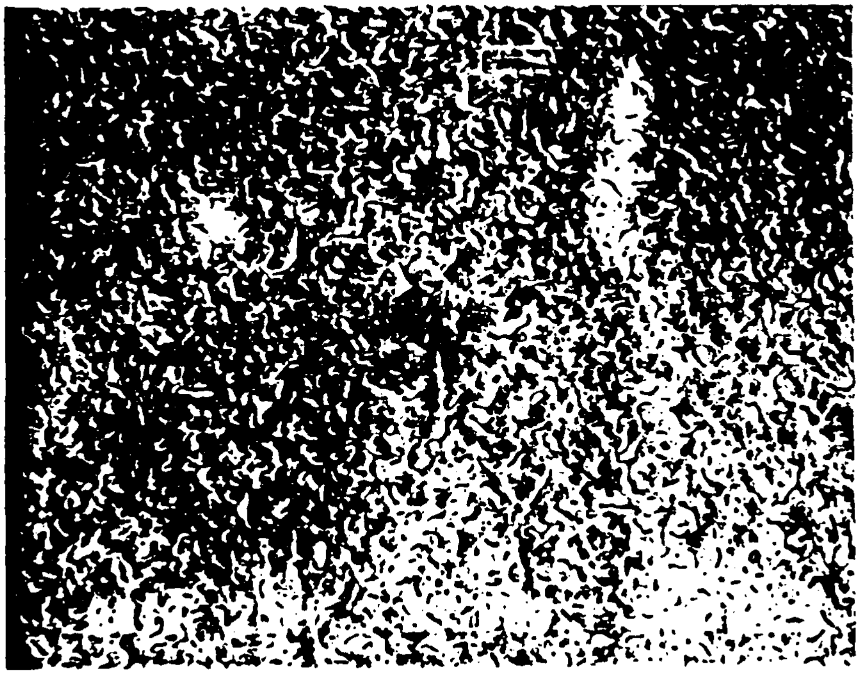

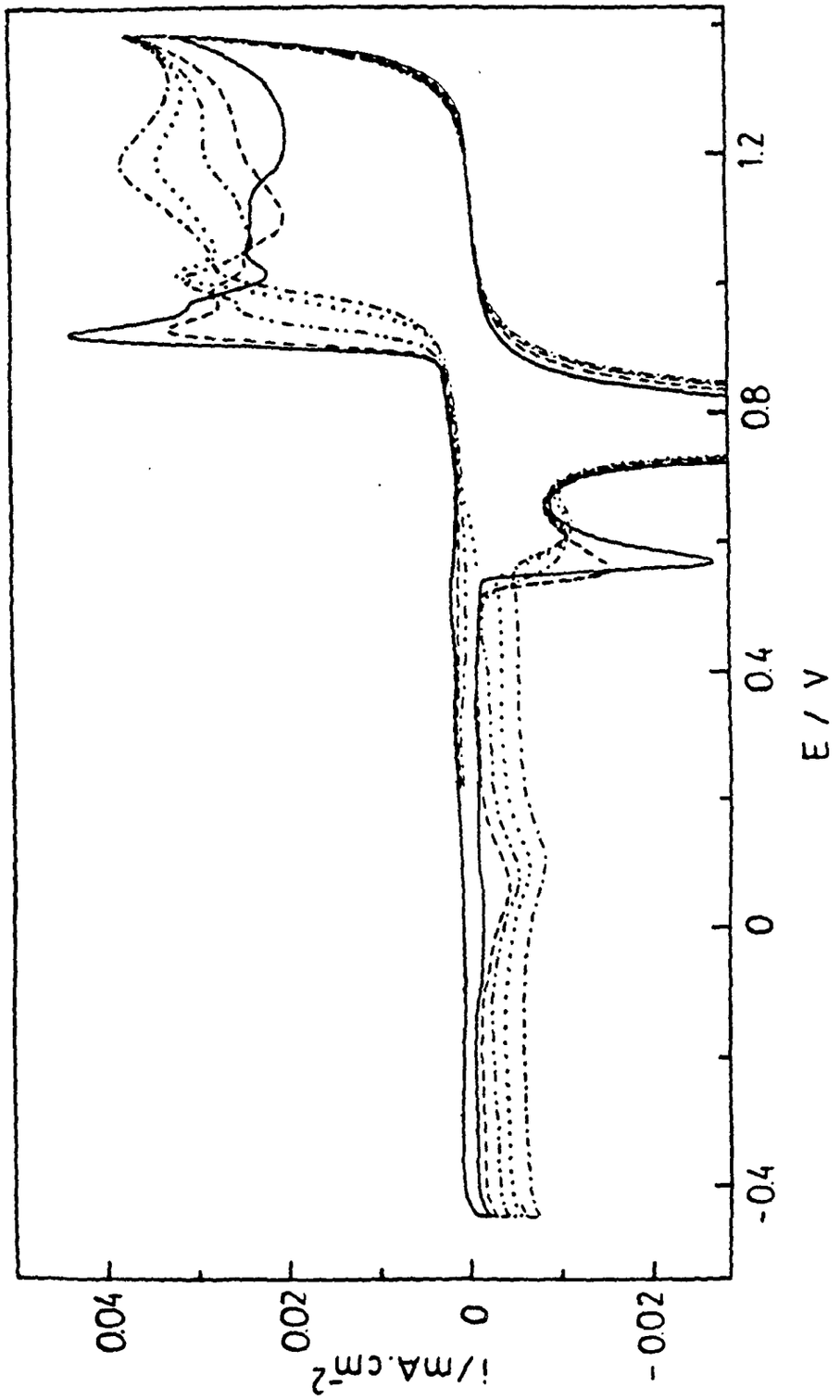

Fig. 15.

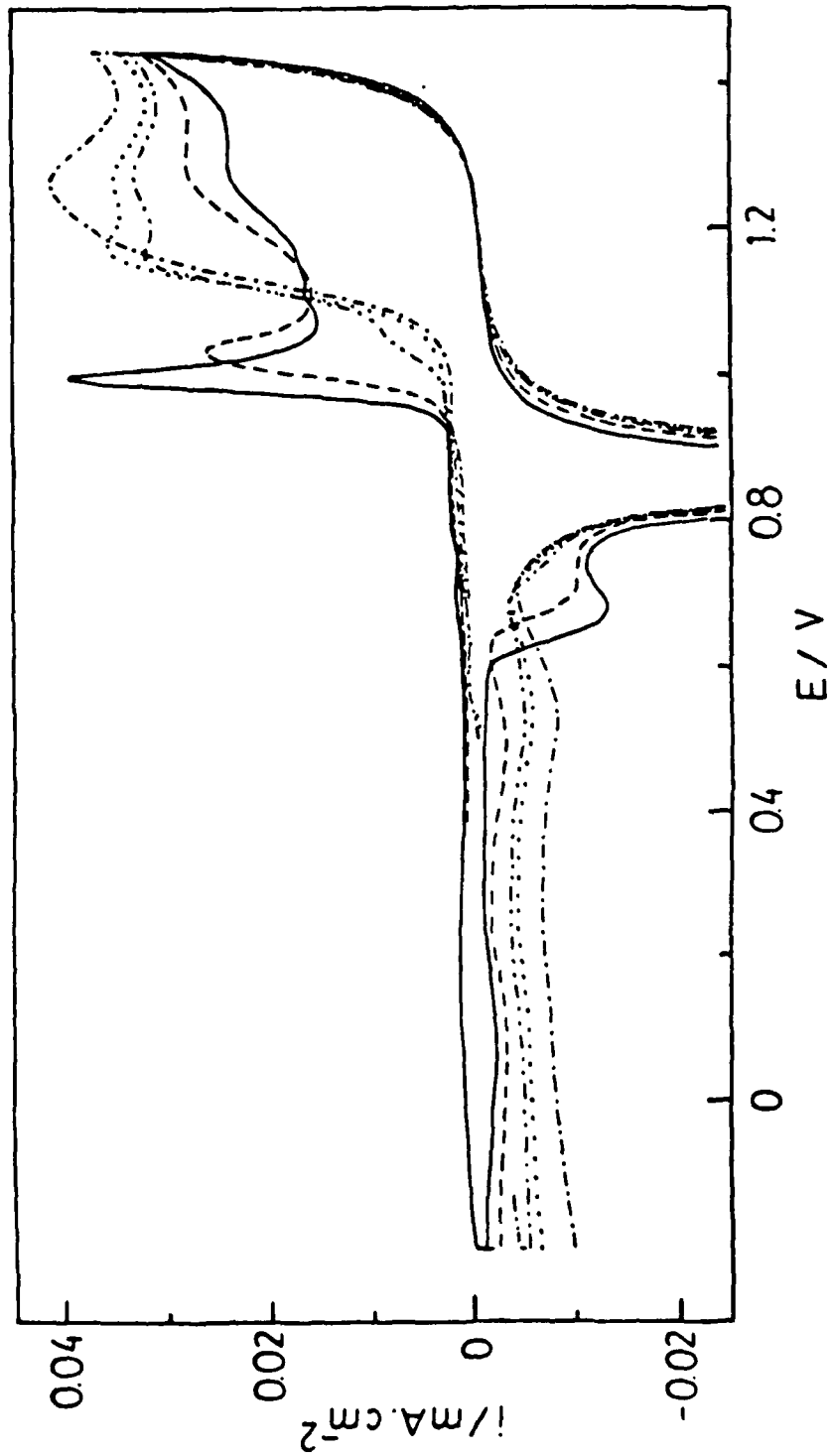

Fig. 16.